# Study on the heat transfer of helium cryostats following loss of insulating vacuum

IOP Conf. Series: Materials Science and Engineering **502** (2019) 012170 doi:10.1088/1757-899X/502/1/012170

# Study on the heat transfer of helium cryostats following loss of insulating vacuum

**C Weber[1,2], A Henriques[3] and S Grohmann[1,2]**

[1] Karlsruhe Institute of Technology (KIT), Institute for Technical Physics, Hermann-von-Helmholtz-Platz 1, 76344 Eggenstein-Leopoldshafen, Germany
[2] KIT, Institute for Thermodynamics and Refrigeration, Kaiserstrasse 12, 76131 Karlsruhe, Germany
[3] European Organization for Nuclear Research (CERN), CH-1211, Geneva 23, Switzerland

E-mail: christina.weber@kit.edu

**Abstract.** The dimensioning of pressure relief devices (PRD) for helium cryostats requires detailed knowledge of the pressure increase during incidents. In case of the loss of insulating vacuum (LIV), this is induced by heat input due to deposition of atmospheric air on the surface of the helium vessel. Instead of considering the process dynamics, the dimensioning of PRD according to established standards is based on constant heat flux values, yielding potential oversizing. However, the heat flux depends on the rate of air reaching the cold surface, the thermal capacitance of and the heat transfer resistance inside the helium vessel, which are temperature-/time-dependent.

In order to improve the theoretical basis for the dimensioning of cryogenic PRD, this work presents a one-dimensional heat transfer model to calculate the heat flux dynamics based on dominating physical mechanisms. The results are compared with experimental data measured in the cryogenic safety test facility PICARD.

## 1. Introduction

The sizing of cryogenic PRD according to established standards is often based on constant heat flux values. However, venting experiments conducted on the cryogenic safety test facility PICARD[1] [1–3] have shown that neglecting the process dynamics may result in oversized PRD. Hence, a modelling approach for sizing of cryogenic PRD that considers the process dynamics after LIV is introduced in [4, 5]. The dynamic venting process is depicted in figure 1(a), where atmospheric air flows through an orifice into the evacuated space and deposits on the surface of the cryogenic vessel. The resulting deposition heat is transferred through the wall to the helium inside the cryogenic vessel, where it causes an isochoric temperature and pressure increase until the relieving pressure of the PRD is reached. The PRD opens and releases the discharge mass flow rate at constant pressure while the temperature evolution depends on the relieving pressure and the filling level. It increases either at supercritical pressure or at subcritical pressure if only gaseous helium is stored in the cryostat. It stays constant at subcritical pressure and a liquid level, because of the latent heat of vaporization.

Based on venting experiments at PICARD, the deposition process of the venting fluid, i.e. the fluid flowing into the insulating vacuum, on the cryogenic surface is already modelled in [6],

[1] **P**ressure **I**ncrease in **C**ryostats and **A**nalysis of **R**elief **D**evices.

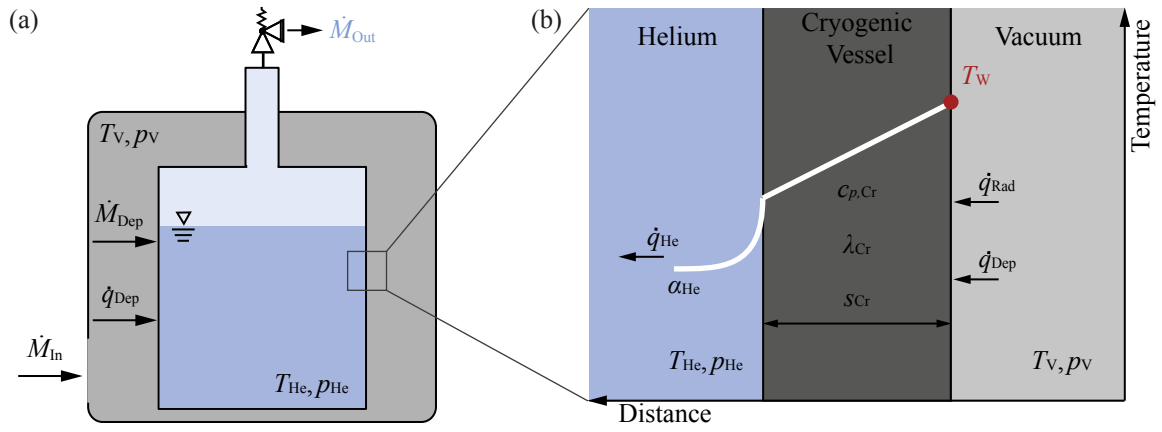


**Figure 1.** Schematic representation of a cryostat with the main time-dependent variables (a), and a zoom into the schematic temperature profile (b) between the vacuum space and the Helium inside the cryogenic vessel with the heat transfer coefficient $\alpha$, the thermal conductivity $\lambda$ and all relevant heat flux $\dot{q}$.

including an empirical fit of measured wall temperature data. However, the transient heat transfer process inside the cryogenic vessel has not been implemented so far. Therefore, the dynamic model in [6] is adapted and extended considering also the heat conduction in the vessel wall and the heat convection to the cryogenic fluid.

The improved transient heat transfer model is explained in section 2 of this paper. The results of the model are presented in section 3 in comparison to experimental data obtained from PICARD. Section 4 gives a summary and an outlook.

## 2. Simulation approach for the heat transfer

The temperature profile between the vacuum space and the helium is schematically depicted in figure 1(b). In order to combine the air deposition in the vacuum space, the heat conduction in the cryogenic vessel and the convection in the helium, the time-dependent wall temperature profile on the outer surface of the cryogenic vessel $T_W$ is calculated by the one-dimensional transient heat equation

$$\frac{\mathrm{d}T_W}{\mathrm{d}t} = \frac{A_{Cr}}{c_{p,Cr} \cdot M_{Cr}} \cdot (\dot{q}_{Rad} + \dot{q}_{Dep} - \dot{q}_{He}) \tag{1}$$

where $A_{Cr}$ is the outer surface of the cryogenic vessel, $c_{p,Cr}$ is the specific heat capacity of the vessel wall at average vessel temperature, $M_{Cr}$ is the mass of the wall, $\dot{q}_{Rad}$ is the heat flux due to thermal radiation, $\dot{q}_{Dep}$ is the deposition heat flux and $\dot{q}_{He}$ is the heat flux transferred to helium. A convective heat transfer resistance in the vacuum space is not considered, as it is negligible compared to the deposition heat.

*Thermal radiation*: The Stefan-Boltzmann equation for a concentric annular gap provides the thermal radiation heat flux

$$\dot{q}_{Rad} = \frac{\sigma}{\frac{1}{\epsilon_V} + \frac{A_V}{A_{Cr}} \cdot \left(\frac{1}{\epsilon_{Cr}} - 1\right)} \cdot \left(T_V^4 - T_W^4\right) \tag{2}$$

where $\sigma$ is the Stefan-Boltzmann constant, $T_V$ is the temperature and $A_V$ is the inner surface of the vacuum vessel having an emissivity $\epsilon_V$ of oxidized stainless steel. For the emissivity $\epsilon_{Cr}$

of the cryogenic vessel values for either electro-polished stainless steel or for the ice layer after LIV [7] are assumed.

*Deposition*: The deposition heat flux $\dot{q}_{\mathrm{Dep}}$ can be derived by multiplying the deposition mass flow rate $\dot{M}_{\mathrm{Dep}}$ with the enthalpy difference from ambient to the wall conditions assuming that the deposition layer is uniformly formed over the entire cryogenic surface, although the leak is localized.

$$\dot{q}_{\mathrm{Dep}} = \frac{\dot{M}_{\mathrm{Dep}}}{A_{\mathrm{Cr}}} \cdot \left( h\left(T_{\mathrm{Amb}}, p_{\mathrm{V}}\right) - h\left(T_{\mathrm{W}}, p_{\mathrm{V}}\right) \right) \tag{3}$$

where $h$ is the enthalpy, $p_{\mathrm{V}}$ is the pressure in the vacuum space and $T_{\mathrm{Amb}}$ is the ambient temperature. $\dot{M}_{\mathrm{Dep}}$ itself is calculated by means of the Hertz-Knudsen diffusion equation, a kinetic theory that is commonly used to describe cryopumping [8]

$$\dot{M}_{\mathrm{Dep}} = A_{\mathrm{Cr}} \cdot \alpha_{\mathrm{T}} \cdot \frac{1}{\sqrt{2 \cdot \pi \cdot R_{\mathrm{V}}}} \cdot \left( \alpha_{\mathrm{C}} \cdot \frac{p_{\mathrm{V}}}{\sqrt{T_{\mathrm{Amb}}}} - \alpha_{\mathrm{E}} \cdot \frac{p_{\mathrm{V,s}}\left(T_{\mathrm{W}}\right)}{\sqrt{T_{\mathrm{W}}}} \right) \tag{4}$$

where $\alpha_{\mathrm{T}}$ is the transmission coefficient describing the probability of molecules passing through obstacles, $\alpha_{\mathrm{C}}$ is the condensation coefficient defining the probability of molecules being deposited on the cold surface, $\alpha_{\mathrm{E}}$ is the evaporation coefficient defining the probability of molecules leaving the cold surface, $R_{\mathrm{V}}$ is the specific ideal gas constant of the venting fluid and $p_{\mathrm{V,s}}$ is its saturation pressure at wall temperature. A general derivation and the values of these coefficients are given in [6]. In contrast to [6] though, $\alpha_{\mathrm{C}}$ and $\alpha_{\mathrm{E}}$ are fitted to the Clausius Clapeyron equation between 20 K and the triple point temperature, as these coefficients are - among other physical variables - a function of the saturation pressure.

*Wall conduction and heat transfer to Helium*: The heat flux to the helium is calculated by application of the Fourier equation

$$\dot{q}_{\mathrm{He}} = \left( \frac{s_{\mathrm{Cr}}}{\lambda_{\mathrm{Cr}}} + \frac{1}{\alpha_{\mathrm{He}}} \right)^{-1} \cdot \left( T_{\mathrm{W}} - T_{\mathrm{He}} \right) \tag{5}$$

where $\lambda_{\mathrm{Cr}}$ is the thermal conductivity of the cryogenic vessel at average temperature, $s_{\mathrm{Cr}}$ is the thickness of the vessel wall, $\alpha_{\mathrm{He}}$ is the heat transfer coefficient to the helium and $T_{\mathrm{He}}$ is the average helium bulk temperature. Stratification, temperature gradients in the bulk and transition times for the establishment of two phase heat transfer regimes are not considered. The latter is a reasonable assumption in this application, since the transition times are less than 0.1 s [9].

$\alpha_{\mathrm{He}}$ depends on the thermodynamic state of helium. Before reaching the thermodynamic critical pressure, either nucleate or film boiling occurs [9], depending on the heat flux[2]. The correlation of Kutateladze [10] is used for the nucleate boiling regime and the correlation of Breen and Westwater [11] for the film boiling regime. The mean error of the Kutateladze correlation applied to measured helium data is given in [12] as 12.9 %. At pressures above the thermodynamic critical pressure, a correlation for free convection on a semi-infinite plate of constant temperature in an infinite medium is used [13]. The standard deviation of this correlation is 5.3 %.

*Numerical solution*: The initial-value problem for the ordinary first-order differential equation system is solved using a pair of (4,3) explicit Runge-Kutta formula [14] in the computer algebra system Mathematica [15]. A discrete proportional integrate (PI) step-size controller is used as described in [16] in order to overcome the problem of oscillating step-size sequences that typically

[2] The minimum film boiling heat flux of helium is assumed to be $0.3\,\mathrm{Wcm^{-2}}$ [9].

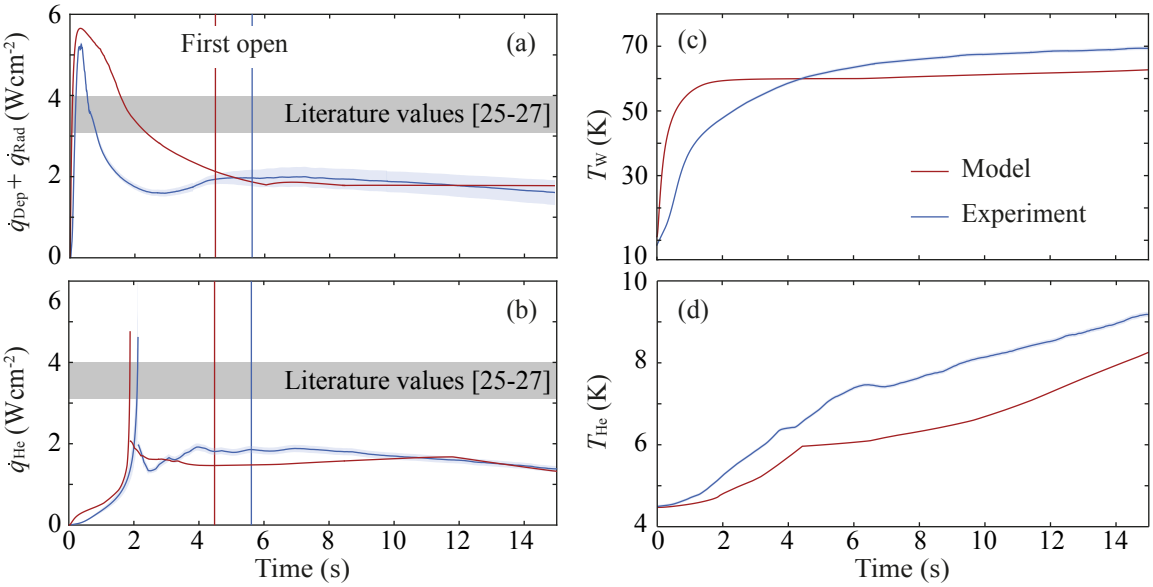


**Figure 2.** Modelled and measured profiles of the deposition heat flux (a) the heat flux transferred to helium (b), the wall temperature (c) and the helium temperature increase (d). The results of the model are depicted in red, while the experimental data are shown in blue with their measurement uncertainties [24] in lighter blue. The range of constant literature values is displayed in grey.

appears when stiffness is encountered. The fluid properties of the venting and cryogenic fluid are implemented as functions of temperature and pressure via the REFPROP Database [17–23].

## 3. Discussion

In this section, the presented model is compared to experimental data obtained from PICARD. The resulting heat flux profiles to and from the cryogenic vessel, as well as the wall and the helium temperature increase during LIV are shown in figure 2. The experimental parameters delivering the initial and boundary conditions for the model are as follows: 6 bar(g) set pressure of the PRD, 60 % initial filling level and 30 mm diameter of the venting orifice.

Figure 2(a) shows a complex shape of $\dot{q}_{\mathrm{Dep}} + \dot{q}_{\mathrm{Rad}}$, which is explained by the dependence of $\alpha_{\mathrm{C}}$ and $\alpha_{\mathrm{E}}$ on the vacuum pressure (cf. [6]). Despite some difference in between $2 - 4\,\mathrm{s}$, the modelling result is in good agreement with the experimental data. The peak value of $5.6\,\mathrm{Wcm^{-2}}$ is calculated with 8 % deviation, while the heat flux at the first opening of the PRD ($2.1\,\mathrm{Wcm^{-2}}$) that is relevant for sizing is calculated within the measurement uncertainty at this time.

The peak of $\dot{q}_{\mathrm{He}}$ shown in figure 2(b) is time-shifted, as the heat transfer to the helium is lower due to film boiling than the thermal conduction in the wall in the first seconds. However, the heat conduction in the wall is not negligible as confirmed by a Biot-number[3] of $0.1 < Bi < 1$. For a short duration of time between $2 - 2.3\,\mathrm{s}$, the dominating heat transfer resistance changes, as $\alpha_{\mathrm{He}}$ increase due to fluid property data in the vicinity of the critical point. Beyond the critical point of helium, the heat transfer coefficient and thus the heat flux drop due to the change in the heat transfer mechanism to free convection. At this time, $\dot{q}_{\mathrm{He}}$ is about 20 % lower than $\dot{q}_{\mathrm{Dep}}$ and the heat transfer resistance of helium is higher than the thermal conduction resistance again ($0.1 < Bi < 1$).

[3] The Biot-number defines the ratio of the thermal conductive resistance to the thermal transfer resistance.

In accordance with the difference between in- and out-flowing heat fluxes, the modelled wall temperature $T_W$ in figure 2(c), increases faster than the measured one up to the first opening of the PRD, but stagnates at 10 % below the measured value. Neglecting the isolation effect of the ice layer due to uncertain material property data of the ice may be a reason for this deviation.

The the lower modelled than measured $\dot{q}_{He}$ explains also the flatter helium temperature increase after reaching the critical pressure, shown in figure 2(d). An additional reason for the underestimation of the helium temperature can be due to stratification inside the helium.

## 4. Summary and outlook

In this paper, an approach on modelling the heat transfer of helium cryostats following loss of insulating vacuum without any empirical parametrisation is introduced. Experimental data obtained from the cryogenic safety test facility PICARD are well predicted with the present model. Modelled and measured heat flux data relevant for sizing of PRD are lower than the established constant values from literature [25–27].

As the heat transfer is mostly affected by the convection to helium, additional helium heat transfer correlation will be tested and the effect of stratification inside the helium may have to be considered. In future work, the model will be compared to different experimental conditions and its reliability and uncertainty evaluated.

## References

[1] Heidt C, Schön H, Stamm M and Grohmann S 2015 *IOP CONF. SER. MATER. SCI. ENG* **101** 012161
[2] Heidt C, Henriques A, Stamm M and Grohmann S 2017 *IOP CONF. SER. MATER. SCI. ENG* **171** 012044
[3] Weber C, Henriques A, Zoller C and Grohmann S 2017 *IOP CONF. SER. MATER. SCI. ENG* **278** 012169
[4] Chorowski M, Fydrych J, Polinski J and Süßer M 2006 *PROC INT CRYOG ENG CONF* **21** 141–144
[5] Heidt C, Grohmann S and Süßer M 2014 *Adv. Cryog. Eng.* **1573** 1574–1580
[6] Zoller C 2018, Karlsruhe *Ph.D. Thesis. Experimental investigation and modelling of incidents in liquid helium cryostats*
[7] Verein Deutscher Ingenieure 2010 *VDI Heat Atlas* 2nd ed (Springer)
[8] Haefer R A 1989 *Cryopumping: theory and practice* 1st ed Monographs on cryogenics, 4 (Clarendon Pr.)
[9] Van Sciver S W 2012 *Helium Cryogenics* 2nd ed Int. Cryogenics Monogr. Ser. (Springer)
[10] Kutateladze S S 1951 *Izvestia Akademia Nauk Otdelenie Tekhnicheski Nauk* **4** 529–536
[11] Breen B P and Westwater J W 1962 *Chem. Eng. Prog.* **58** 67
[12] Bewilogua L, Knöner R and Vinzelberg H 1975 *Cryogenics* **15** 121–125
[13] Hilal M A and Boom R W 1979 *Int. J. Heat Mass Transfer* **23** 697–705
[14] Feldberg E 1969 *NASA TP, R-315*
[15] Inc W R 2018 Mathematica, Version 11.3
[16] Gustafsson K 1991 *ACM Trans. Math. Softw.* **17** 533–554
[17] Lemmon E W, Huber M L and McLinden M O 2013 Refprop. Version 9.1
[18] Ortiz Vega D O 2013, Texas *Ph.D. Thesis. A new wide range equation of state for helium-4*
[19] Lemmon E W, Jacobsen R T, Penoncello S G and Friend D G 2000 *J Phys Chem Ref Data* **29** 331–385
[20] Span R, Lemmon E W, Jacobsen R T, Wagner W and Yokozeki A 2000 *J Phys Chem Ref Data* **29** 1361–1433
[21] Schmidt R and Wagner W 1985 *Fluid Phase Equilib* **19** 175–200
[22] Tegeler C, Span R and Wagner W 1999 *J Phys Chem Ref Data* **28** 779–850
[23] Wagner W and Pru A 2002 *J Phys Chem Ref Data* **31** 387–535
[24] Bureau International des Poids et Mesures 2008 Evaluation of measurement data – guide to the expression of uncertainty in measurement
[25] Lehmann W and Zahn G 1978 *Proc. Int. Cryog. Eng. Conf* **7** 569–579
[26] Cavallari G, Gorine I, Güsewell D and Stierlin R 1989 *Proc. 4th Workshop on RF Supercon.* **1** 781–803
[27] Harisson S 2002 *IEEE T. Appl. Supercon. 12* **12** 1343–1346

## Acknowledgements

The authors would like to acknowledge the support from the CERN Knowledge Transfer Group and the KIT Legal Department as well as the Karlsruhe School of Elementary Particle and Astroparticle Physics: Science and Technology (KSETA).